

THE GALANTE PHOTOMETRIC SYSTEM

A. Lorenzo-Gutiérrez,^{1*} E. J. Alfaro^{1,3}, J. Maíz Apellániz², R. H. Barbá⁴,
A. Marín-Franch^{3,5}, A. Ederoclite^{3,5,6}, D. Cristóbal-Hornillos^{3,5}, J. Varela^{3,5},
H. Vázquez Ramió^{3,5}, J. Cenarro^{3,5}, D. J. Lennon⁷, and P. García-Lario⁷

¹*Instituto de Astrofísica de Andalucía. Glorieta de la Astronomía s/n. E-18 008 Granada. Spain*

²*Centro de Astrobiología, CSIC-INTA. Campus ESAC. Camino bajo del castillo s/n. E-28 692 Villanueva de la Cañada. Spain*

³*Unidad Asociada CEFCA-IAA. CSIC. Teruel. Spain*

⁴*Universidad de La Serena. La Serena. Chile*

⁵*Centro de Estudios de Física del Cosmos de Aragón. Teruel. Spain*

⁶*Instituto de Astronomia, Geofísica e Ciências Atmosféricas. Universidade de São Paulo. Brazil*

⁷*European Space Agency. ESAC. Camino bajo del castillo s/n. E-28 692 Villanueva de la Cañada. Madrid. Spain*

Accepted XXX. Received YYY; in original form ZZZ

ABSTRACT

This paper describes the characterization of the GALANTE photometric system, a seven intermediate- and narrow-band filter system with a wavelength coverage from 3000 Å to 9000 Å. We describe the photometric system presenting the full sensitivity curve as a product of the filter sensitivity, CCD, telescope mirror, and atmospheric transmission curves, as well as some first- and second-order moments of this sensitivity function. The GALANTE photometric system is composed of four filters from the J-PLUS photometric system, a twelve broad-to-narrow filter system, and three exclusive filters, specifically designed to measure the physical parameters of stars such as effective temperature T_{eff} , $\log(g)$, metallicity, colour excess $E(4405 - 5495)$, and extinction type R_{5495} . Two libraries, the Next Generation Spectral Library (NGSL) and the one presented in Maíz Apellániz & Weiler (2018), have been used to determine the transformation equations between the Sloan Digital Sky Survey (*SDSS*) *ugriz* photometry and the GALANTE photometric system. We will use this transformation to calibrate the zero points of GALANTE images. To this end, a preliminary photometric calibration of GALANTE has been made based on two different *griz* libraries (*SDSS* DR12 and ATLAS All-Sky Stellar Reference Catalog, hereinafter *RefCat2*). A comparison between both zero points is performed leading us to the choice of *RefCat2* as the base catalogue for this calibration, and applied to a field in the Cyg OB2 association.

Key words: techniques: photometric – galaxies: star formation – stars: formation
Cygnus

1 INTRODUCTION

Photometric systems are defined as a set of filters and a detector capable of obtaining information from energy spectral distribution of the objects observed, from which to derive their intrinsic and extrinsic physical properties. The *UBV* system (Johnson & Morgan 1953) based on the spectral response of the human eye (*V*) and the photographic plate (*B*), added a *U* filter to measure the Balmer jump. This addition made it possible to establish a first quantitative re-

lationship between photometric colours and spectral properties. The *UBV* system aimed to take advantage of historical catalogues (visible and photographic) to establish a photometric database with the addition of a new filter. Another 3-band system was defined (Becker 1946) with photographic detectors that disregarded the historical catalogues and focused more on the properties of the emitter than on those of the receiver. On paper, the *RGU* system allowed a better stellar classification than the *UBV*, but the fact that it was based on the photographic plate, with a non-linear response, and depended on transformation equations between the *RGU* and the *UBV* greatly limited its development and

* E-mail: alorenzo@iaa.es

nowadays it is rarely used. Walraven & Walraven (1960) introduced a photometric system with five bands *VBLUW* allowing to measure temperatures for early-type stars. The *W* and *L* bands in the ultraviolet region enabled to estimate the Balmer series in hot stars, in addition with the Johnson's bands. Strömgren (1966) developed a new approach to the photometric system based on narrower filters that not only provided information from the stellar continuum, but also allowed a quantitative measurement of some spectral lines. This fact enabled the possibility of estimating parameters such as metallicity ($[Fe/H]$) for the most common range of temperature we can find in the solar neighborhood. DDO system (McClure & van den Bergh 1968) is another intermediate five-bands system designed to measure temperature and metallicity in late-type stars with a high precision in comparison with previous photometric systems. Recently, Gaia DR2 has provided a whole-sky optical photometric survey using three very broad bands *G*, *G_{BP}*, and *G_{RP}* (Gaia Collaboration et al. 2018; Evans et al. 2018). The coverage, uniformity, and dynamic range of Gaia photometry will undoubtedly be a golden standard for optical photometry in the future. More specifically, Maíz Apellániz & Weiler (2018) (hereinafter MAW) have shown that Gaia DR2 photometry can be calibrated without significant systematic biases and with photometric residuals of one hundredth of a magnitude or better. Since the introduction of the CCD, the development of new photometric systems has halted, reaching its peak with the Sloan Digital Sky Survey (*SDSS*) (Fukugita et al. 1996), which combined the design of a photometric system in five bands, covering the visible range, with an industrial aspect of the observation. Observational strategy in astronomy has undergone a drastic change and the number of large photometric surveys specifically designed to obtain singular information about types of celestial objects has increased significantly.

Examples of this kind of astronomical projects are J-PLUS and J-PAS which are currently being developed in a new observatory in Javalambre (Teruel, Spain) with 2 telescopes of 80 cm and 250 cm. The main scientific objective of J-PAS is cosmological, trying to measure the spectrum of Baryonic Acoustic Oscillations (BAOs) with photometric redshift estimations (Benitez et al. 2014), while J-PLUS was originally planned to be an auxiliary survey for J-PAS calibration purposes (Cenarro et al. 2018). Given the observational restrictions of these programmes in terms of sky darkness and seeing, we designed a new monitoring programme, which we called GALANTE, focused on the brighter stars of the Galactic disk. This programme would be carried out on those clear nights where J-PLUS were not observable.

The GALANTE project is a photometric survey that will cover the Northern Galactic plane defined by $\delta \geq 0^\circ$ and $|b| \leq 3^\circ$. This project uses 7 intermediate+narrow band filters aimed at measuring all stars of that region of the sky with AB magnitudes ≤ 17 . These 7 filters are 4 J-PLUS filters (F348M, F515N, F660N, and F861M) and 3 new customized filters developed by the GALANTE team (F420N, F450N, and F665N). The number, width, and effective wavelength of the filters compose an optimal system to accomplish those objectives proposed by Maíz Apellániz (2017). A Southern version of the GALANTE program has been proposed to be performed with the twin Cerro Tololo 80

cm telescope developed for the S-PLUS project (Saito et al. 2018).

The main goal of this paper is to present the characterization of the 7 GALANTE filters in the optical range, and to establish the first transformation equations between GALANTE and *SDSS*. The GALANTE project covers from 3000 Å to 9000 Å using its 7 filters located at the best place to attain our goal: to obtain more precise information about stellar effective temperatures, gravities, metallicities, and also type of extinction (Maíz Apellániz 2013).

In Section 2, we present the characterization and definition of the GALANTE photometric system. In Section 3, we analyse in detail the set of GALANTE standard stars. Transformation equations between the *SDSS* and the GALANTE photometric system are obtained in Section 4, setting up the comparison between the synthetic magnitudes of 378 stars from the Next Generation Spectral Library (NGSL) plus 122 stars from a new catalogue from MAW in both photometric systems. Next, in Section 5 we estimate zero points from the GALANTE photometry using the *SDSS* and *RefCat2*. Finally, in Section 6 we summarize the results of this paper.

2 THE GALANTE PHOTOMETRIC SYSTEM

2.1 DESCRIPTION

Deriving physical stellar (or galaxy) parameters is the main goal of every photometric system. In our case, we achieve this aim with a new filter set designed to plug some gaps found in previous surveys. The GALANTE photometric system has been defined using 4 J-PLUS filters (Cenarro et al. 2017) and 3 purpose-built filters. This composition of intermediate and narrow band filters covers the optical range from 3000 Å to 9000 Å. This filter set has been selected with a direct goal: deriving stellar effective temperatures for hot stars in an optimal way (Maíz Apellániz & Sota 2008; Maíz Apellániz et al. 2014; Maíz Apellániz & Barbá 2018). We will also be able to obtain the gravity and metallicity (the latter for stars cooler than 10 000 K), allowing us to discriminate between giants, supergiants, dwarfs, and between solar or SMC metallicities.

In Figures 1 and 2 we present the setup of the filters. Figures 1 (a) and (b) show the layout of the J-PLUS and GALANTE filters respectively, leaning on the Vega spectrum. Note that in this case we only plot the transmission curves of the filters, allowing to the reader a visual location of each one. Focusing on GALANTE, Figure 1 (b) plots the configuration of the selected GALANTE filters, which enable us to measure the key zones in the spectra to derive physical parameters. In Figure 2 we plot the response functions of the J-PLUS and the GALANTE photometric system filters. In discontinuous grey we represent the response curve of the CCD and mirror, while discontinuous green is the CCD, mirror and atmospheric transmission at 1.3 air mass curve. The *SDSS* response curves are represented in continuous black, and the other continuous curves are the GALANTE and J-PLUS filter response curves convolved with CCD, mirror and atmospheric transmission at 1.3 air mass. Using Figure 3, we can also explain the function of each GALANTE filter with greater accuracy. Filter F348M is a *u*-like filter disposed to measure the continuum from the left of the Balmer jump.

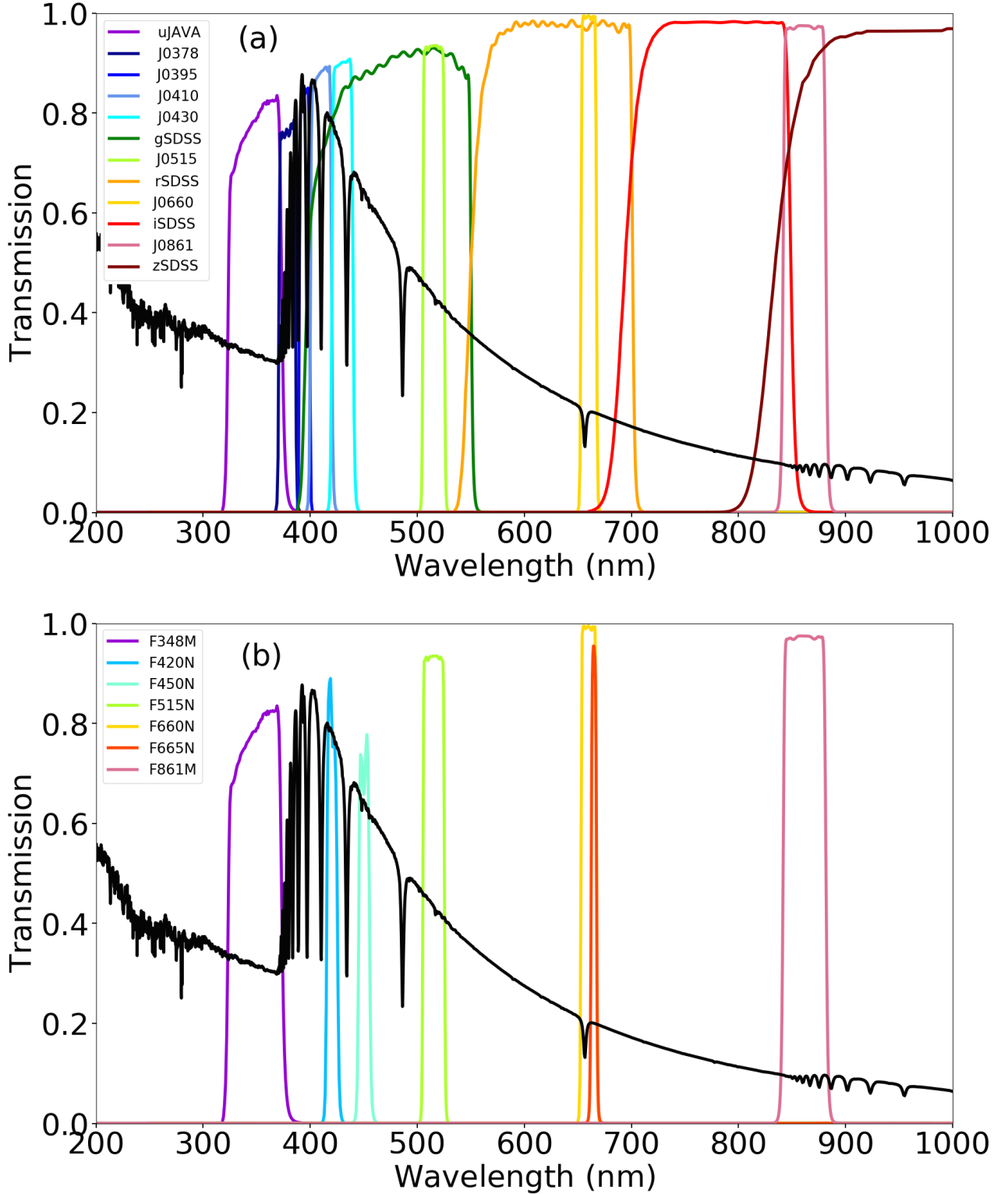


Figure 1. Response functions of the J-PLUS and the GALANTE photometric system filters. In both pictures we only took into account filter transmission curves to visualize their positions. Figure (a) represents the Vega spectrum superimposed onto J-PLUS filters transmission curves. Figure (b) represents the Vega spectrum superimposed onto GALANTE filters transmission curves. To make the graphic possible, the flux of Vega has been normalized and scaled properly.

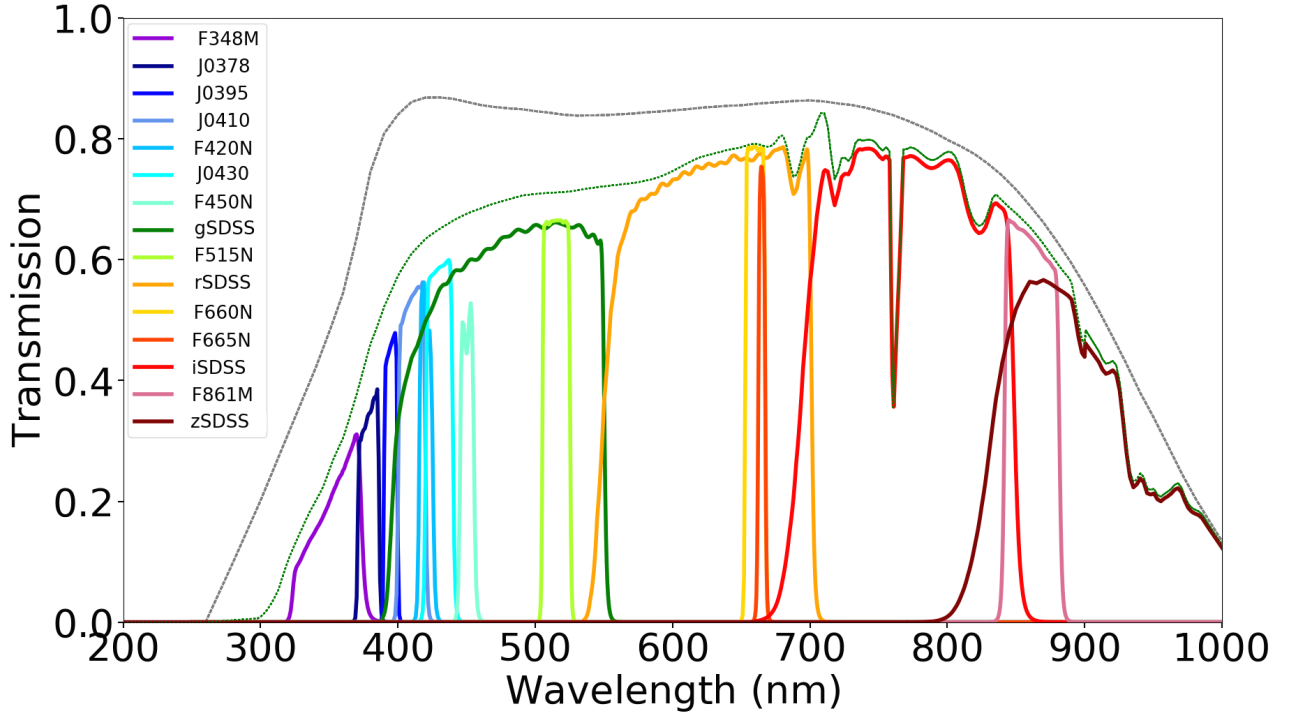


Figure 2. Response functions of the J-PLUS and the GALANTE photometric system filters. In discontinuous grey we represent the response curve of the CCD and mirror, while discontinuous green is the CCD, mirror and atmospheric transmission at 1.3 air mass curve. The *SDSS* response curves are represented by thick colored lines with the other continuous curves are the GALANTE and J-PLUS filter response curves convolved with CCD, mirror and atmospheric transmission at 1.3 air mass.

We can combine this one with F420N and F450N to measure the Balmer jump on both sides and derive the T_{eff} of stars. Both filters of our design, F420N and F450N, are the most original (compared to other large-scale recent photometric surveys) of the setup. They have been created to fill the gaps between $H\delta$ and $H\gamma$ and between $H\gamma$ and $H\beta$ respectively. These are the bluest wide regions of the spectrum to the right of the Balmer jump without absorption lines and they provide a measurement of the blue continuum. Another J-PLUS filter used in GALANTE is F515N. It is a Strömgren y -like filter positioned in a region free of lines. It can be seen as a V filter for this survey. The next pair of filters, namely F660N (from J-PLUS) and F665N (own-design), allow us to measure the red continuum, estimate the gravity of hot stars, and flag objects with $H\alpha$ emission. These are two narrow filters centered on $H\alpha$. Specifically, F660N includes the line and F665N just the continuum. The last filter is F861M (from J-PLUS). This is an intermediate filter in the Calcium triplet. It will be used as a detection filter, to obtain the maximum number of stars. We can also use a combination of some GALANTE filters, for a fixed metallicity and extinction law, to obtain effective temperature T_{eff} independently of reddening. Figure 4 shows a GALANTE colour-colour diagram using F348M, F420N, F450N, and F515N for stars from 4000 K to 40 000 K with different colour excess $E(4405 - 5495)$ and extinction type R_{5495} .

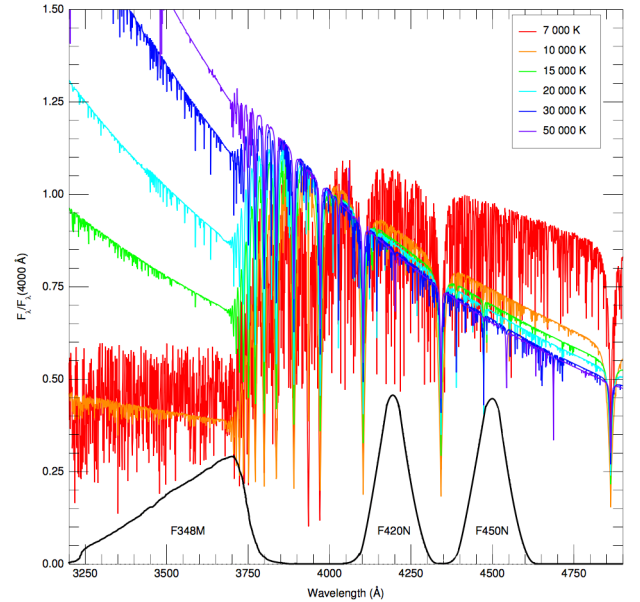


Figure 3. SEDs for main-sequence hot stars normalized to the flux at 4000 Å and sensitivity curves of the three bluest GALANTE filters. F420N and F450N have been approximated by gaussians while F348M has been represented by a rectangular filter with a linear atmospheric absorption effect. Note how F348M measures the continuum to the left of the Balmer jump while F420N and F450N are located at the gaps between the Balmer lines.

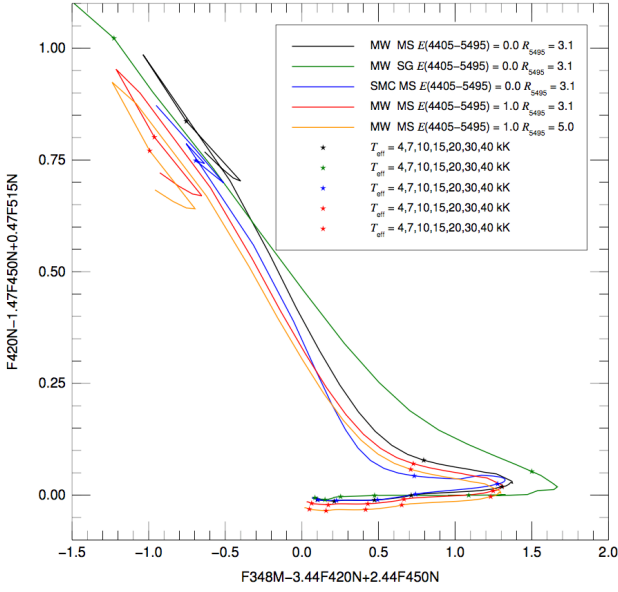


Figure 4. Bracket-like diagram using the GALANTE filter set. It shows how, for a fixed metallicity and extinction law, it is possible to classify the stars by T_{eff} independently of reddening.

2.2 CHARACTERIZATION

With our GALANTE configuration, we can describe the system using a response curve defined by the three different transmission curves. Figure 1 shows the graphic representation of the optical GALANTE+J-PLUS photometric systems. In order to characterize the GALANTE filter set, we need to describe the filter with some quantitative parameters such as: their isophotal wavelengths, wavelength-weighted average, frequency-weighted average, effective wavelength, root mean square, effective band width, and flux sensitivity. Thus, we define the total response of a photometric system (S_λ) by

$$S_\lambda = T_t(\lambda)T_f(\lambda)T_a(\lambda) \quad (1)$$

Here T_t is the mirror+detector throughput; the filter response transmission is T_f ; and the atmospheric curve transmission at 1.3 airmass is T_a .

If the SED received at the the detector, E_λ , is continuous, and the total response S_λ is also continuous and not negative over a range of wavelengths (Golay 1974), using Equation 1 and the mean value theorem, we can say that λ_i exists and has the form of:

$$E_{\lambda_i} \int_{\lambda_a}^{\lambda_b} S_\lambda d\lambda = \int_{\lambda_a}^{\lambda_b} E_\lambda S_\lambda d\lambda \quad (2)$$

If we rearrange this equation:

$$E_{\lambda_i} = \langle E_\lambda \rangle = \frac{\int_{\lambda_a}^{\lambda_b} E_\lambda S_\lambda d\lambda}{\int_{\lambda_a}^{\lambda_b} S_\lambda d\lambda} \quad (3)$$

where λ_i is the *isophotal wavelength* and $\langle E_\lambda \rangle$ is the mean value of the intrinsic flux above the atmosphere (see also

Tokunaga & Vacca 2005). We show the isophotal wavelengths for Vega using GALANTE+J-PLUS filters in Table 2. These values were obtained from Equation 3 using the Vega spectrum provided by Bohlin (2007) and available at ftp://ftp.stsci.edu/cdbs/calspec/alpha_lyr_stis_003.fits, for the optical range.

The isophotal wavelength depends on the Spectral Energy Distribution (SED); thus, for each kind of star it will be different for the same filter. Then we need to define several photometric parameters, as shown in Table 1, depending only on the photometric system.

We calculated all those parameters and they are collected in Table 2 and Table 3 in order to give a precise description of the GALANTE and J-PLUS filters. Note that the GALANTE photometric system is composed of F348M, F420N, F450N, F515N, F660N, F665N, and F861M. In this way, we put all the 7 GALANTE filters together in Table 2, adopting a different nomenclature, but some of them are the same filters used in J-PLUS. The first column shows their GALANTE names, while the second one shows the J-PLUS nomenclature.

3 STANDARD STARS SYSTEM

To obtain the GALANTE transformation equations, we use two observational catalogues: NGSL (Gregg et al. 2006) and MAW (Maíz Apellániz & Weiler 2018). The NGSL library comprises of 378 high signal-to-noise stellar spectra. This catalogue has all these stars with a good spectral resolution, all of them homogeneously flux calibrated, covering a large range of spectral types, gravities, and metallicities ($3100 \text{ K} \leq T_{\text{eff}} \leq 32500 \text{ K}$, $0.45 \leq \log(g) \leq 5.4$, $-2.0 \leq [\text{Fe}/\text{H}] \leq 0.5$ and a range of $E(B-V)$ from 0 to 0.75). The wavelength coverage of these spectra is from 2000 \AA to $10\,200 \text{ \AA}$ at resolution $R \sim 1000$.

We also take advantage of the new MAW library of 122 objects observed with HST/STIS spectrophotometry. This selection provides us a library of hot stars with significant extinction plus three M dwarfs, thus covering a wide range of colours that can be defined by their intrinsic colour or their reddening.

These two catalogues complement each other in the sense of covering the whole range of stellar temperatures observed in an ample grade of extinction, in such a way that the same colour, for example ($g-r$), could represent an unreddened intermediate-type star or a very reddened early-type object. This complementarity will be crucial when estimating the transformation equations between GALANTE and SDSS systems.

The AB magnitude system defined by (Oke & Gunn 1983) has been chosen to set the magnitudes in the GALANTE photometric system.

$$AB_V = -2.5 \cdot \log f_\nu - 48.60 \quad (4)$$

where f_ν is the flux per unit frequency of an object in $\text{erg cm}^{-2} \text{ s}^{-1} \text{ Hz}^{-1}$. The constant is extrated setting AB magnitude equal to V magnitude of the Vega flux:

$$48.60 = -2.5 \cdot \log F_0 \quad (5)$$

Table 1. Representative Photometric Parameters.

Parameter	Description	Formula
λ_m	Wavelength-weighted average	$\int \frac{\lambda S_\lambda d\lambda}{S_\lambda d\lambda}$
ν_m	Frequency-weighted average	$\int \frac{\nu S_\nu d(\ln \nu)}{S_\nu d(\ln \nu)}$
λ_{eff}	Effective wavelength	$\exp \left[\frac{\int d(\ln \nu) S_\nu \ln \lambda}{\int d(\ln \nu) S_\nu} \right]$
σ	Root Mean Square (rms) of the filters	$\sqrt{\frac{\int d(\ln \nu) S_\nu \left[\ln \left(\frac{\lambda}{\lambda_{\text{eff}}} \right) \right]^2}{\int d(\ln \nu) S_\nu}}$
δ	Effective band width (with n=0)	$2(2\ln 2)^{\frac{1}{2}} \sigma \lambda_{\text{eff}}$
Q	Flux sensitivity	$\int d(\ln \nu) S_\nu$

Table 2. Representative Parameters of the filters of the GALANTE Photometric System.

Filter	m_{AB} (Vega)	E_{λ_i} (Vega)	λ_{iso}	λ_m	$c\nu_m^{-1}$	λ_{eff}	σ	δ	Q	
GALANTE	J-PLUS	(mag)	($\text{erg s}^{-1} \text{cm}^{-2} \text{\AA}^{-1}$)	(nm)	(nm)	(nm)	(nm)			
F348M	uJAVA	1.071	3.215e-09	354.6	354.8	348.5	355.1	0.0422	35.3	0.0286
F420N		-0.238	8.626e-09	420.5	421.5	421.6	421.9	0.0257	25.6	0.0125
F450N		-0.180	8.502e-09	450.5	451.0	451.0	451.2	0.0185	19.7	0.0116
F515N	J0515	-0.049	4.301e-09	515.2	515.4	515.0	515.5	0.0115	13.9	0.0260
F660N	J0660	0.318	1.981e-09	660.4	660.1	660.0	660.1	0.0066	10.3	0.0175
F665N		0.238	1.979e-09	664.7	665.2	665.2	665.2	0.0174	27.2	0.0061
F861M	J0861	0.560	8.185e-10	861.1	861.2	861.0	861.2	0.0137	27.7	0.0296

Table 3. Representative Parameters of the additional J-PLUS filters.

Filter	m_{AB} (Vega)	E_{λ_i} (Vega)	λ_{iso}	λ_m	$c\nu_m^{-1}$	λ_{eff}	σ	δ	Q
	(mag)	($\text{erg s}^{-1} \text{cm}^{-2} \text{\AA}^{-1}$)	(nm)	(nm)	(nm)	(nm)			
J0378	0.419	6.164e-09	380.1	379.0	378.5	379.1	0.0145	13.0	0.0142
J0395	-0.027	8.052e-09	394.8	395.1	395.0	395.1	0.0102	9.5	0.0115
J0410	-0.165	5.472e-09	410.2	410.4	410.0	410.5	0.0144	14.0	0.0261
J0430	-0.125	7.067e-09	429.7	430.4	430.0	430.4	0.0154	15.6	0.0274
<i>gSDSS</i>	-0.090	5.352e-09	468.7	478.6	480.3	477.0	0.0880	105.3	0.1108
<i>rSDSS</i>	0.163	2.497e-09	618.0	627.6	625.4	622.2	0.0652	104.6	0.1015
<i>iSDSS</i>	0.404	1.301e-09	761.1	769.7	766.8	763.2	0.0592	108.4	0.0766
<i>zSDSS</i>	0.536	9.015e-10	891.7	896.9	911.4	904.9	0.0586	119.8	0.0354

being $F_0 = 3.65 \times 10^{-20} \text{ erg cm}^{-2} \text{ s}^{-1} \text{ Hz}^{-1}$ the flux of Vega at $\lambda = 5480 \text{ \AA}$ used by those authors. Thus we can write the AB_ν magnitudes by:

$$AB_\nu = -2.5 \log \frac{\int f_\nu S_\nu d(\log \nu)}{\int S_\nu d(\log \nu)} - 48.60 \quad (6)$$

where S_ν is the total response of the atmosphere, filter, detector, and mirror transmission. Another way to construct

this magnitude is using the m_{ST} system to derive a m_{AB} equation as a wavelength function. We adopted the formulation proposed by [Casagrande & VandenBerg \(2014\)](#):

$$m_{AB} = -2.5 \cdot \log \frac{\int_{\lambda_i}^{\lambda_f} \lambda f_\lambda S_\lambda d\lambda}{F_0 \cdot c \int_{\lambda_i}^{\lambda_f} \frac{S_\lambda}{\lambda} d\lambda} \quad (7)$$

where c is the speed of light in \AA s^{-1} and f_λ being the flux

per unit of wavelength in $\text{erg cm}^{-2} \text{s}^{-1} \text{\AA}^{-1}$. Equation 7 is used to obtain AB synthetic magnitudes.

The choice of a spectrophotometric library to perform the calibration of a new photometric system is still a topic open to discussion (i.e. Aparicio Villegas et al. 2010; Bessell 2011; Koleva & Vazdekis 2012; Maíz Apellániz & Weiler 2018; Weiler 2018). Maíz Apellániz & Weiler (2018) identify differences of zero-point (ZP) between the MAW and NGS� stellar libraries that can reach up to 0.05 magnitudes for some objects and that on average present an rms of 0.03 magnitudes. However, these differences do not seem to depend on the colour of the stars (Weiler 2018). For the first calibration of GALANTE photometry we will use both libraries although there could be spurious differences of up to 0.05 mag between the two catalogues.

4 GALANTE-SDSS TRANSFORMATION EQUATIONS

Since the GALANTE project is an optical photometric survey in the optical range, we can think of another useful and well known optical survey to transform GALANTE AB magnitudes. This survey is the *SDSS* (Fukugita et al. 1996; Smith et al. 2002), based on an optical photometric system composed of five bands (*ugriz*) in the range from 3000 Å to 11 000 Å. The GALANTE and *SDSS* photometric systems share the same optical wavelength range, thus we will use the NGS� and MAW catalogues to derive transformation equations between both systems.

It is worth noting that both photometric systems are different in several aspects: number of bands and filter bandwidth, as we show in Figure 1. While *SDSS* uses five wide-band filters, GALANTE applies a mix of seven narrow and intermediate-band filter set.

We obtain synthetic photometric GALANTE and *SDSS* AB magnitudes for NGS� and MAW libraries using the response curves shown in Figure 2.

Figure 5 shows a colour-colour diagram for both catalogues. NGS� stars are represented by red dots while MAW stars are shown in blue dots. We also draw a 1 Myr theoretical PARSEC curve with solar metallicity without extinction from <http://stev.oapd.inaf.it/cmd>, isochrones PARSEC release v1.2S + COLIBRI release PR16 (Marigo et al. 2017). Black triangles represent main locus in *SDSS* photometry from Covey et al. (2007). Looking at both catalogues in this figure one can see that the MAW library covers a good number of reddened high-temperature stars, showing a sparse distribution for dwarf late-type and giant stars, whereas the NGS� library covers a wider range of temperature and gravity but is limited in reddening. Lastly, in order to derive GALANTE transformation equations that are as general as possible, we use both catalogues as a single one to better probe the diagram of Figure 5.

We have considered the possibility of modeling these transformations through multilinear fitting with the 4 independent *SDSS* colours (*u-g*, *g-r*, *r-i*, and *i-z*). However, a multilinear analysis where the independent variables are not really stochastically independent can introduce significant biases. For this reason, we first analysed the covariance matrix of both catalogues, which are shown below (Equation 8 and 9), where we see a high correlation between these

4 colours. Therefore, we have decided to use only a linear fitting to a colour. Equation 10 shows the general case, where *i* indicates the GALANTE bands, *k* the *SDSS* band, and *j* specifies the *SDSS* colour used. To select the best fit, we have considered all the possible combinations of *SDSS* colours, choosing the one that shows a lower BIC parameter.

$$NGSL_{corr} = \begin{pmatrix} 1.000 & 0.918 & 0.772 & 0.797 \\ 0.918 & 1.000 & 0.893 & 0.908 \\ 0.772 & 0.893 & 1.000 & 0.991 \\ 0.797 & 0.908 & 0.991 & 1.000 \end{pmatrix} \quad (8)$$

$$MAW_{corr} = \begin{pmatrix} 1.000 & 0.842 & 0.810 & 0.826 \\ 0.842 & 1.000 & 0.887 & 0.931 \\ 0.810 & 0.887 & 1.000 & 0.983 \\ 0.826 & 0.931 & 0.983 & 1.000 \end{pmatrix} \quad (9)$$

$$Gal_i - SDSS_k = c_{ijk} \cdot (SDSS_j - SDSS_{j+1}) + d_{ijk} \quad (10)$$

We obtain the transformation equations between the *SDSS* and the GALANTE photometric systems (and vice versa) using the following procedure. To do this, we use AB GALANTE synthetic magnitudes as dependent and the *SDSS* synthetic magnitudes as independent variables. We obtain magnitudes in the GALANTE photometric system from *SDSS* using the statistical package *Statsmodels* in **Python** for this linear fitting. This algorithm provides a goodness of fit parameter called Bayesian Information Criterion (BIC), defined as

$$BIC = -2 \cdot \ln L + f \cdot \ln(n) \quad (11)$$

where *n* is the sample size of the catalogue, *f* is the number of free parameters, and *L* is the likelihood. This parameter has been chosen to select the best solution, choosing that fitting with a lower BIC for each *SDSS* colour. Equation 12 summarizes the transformation equations from *SDSS* DR12 to GALANTE photometry.

$$\begin{aligned} F348M - u &= 0.149; \text{ rms} = 0.067 \\ F420N - g &= 0.317 \cdot (u-r) - 0.182; \text{ rms} = 0.068 \\ F450N - g &= 0.125 \cdot (g-i); \text{ rms} = 0.027 \\ F515N - g &= -0.300 \cdot (g-r) - 0.032; \text{ rms} = 0.028 \\ F660N - r &= -0.134 \cdot (g-z) + 0.040; \text{ rms} = 0.019 \\ F665N - r &= -0.138 \cdot (g-i) + 0.010; \text{ rms} = 0.009 \\ F861M - z &= 0.047 \cdot (r-z) + 0.005; \text{ rms} = 0.008 \end{aligned} \quad (12)$$

After this fitting we plot the residuals versus (*g-r*) in Figure 6. The residuals have been split for each library. For (*g-r*) < 0.3, the high-reddened hot stars (blue points) are well differentiated from the distribution of red points representing less-reddened intermediate-type stars, especially for the F348M, F420N, F450N, and F660N filters.

If we take a look at these figures, F348M-*u*, and F420N-*g* residuals are more scattered than for the other filters, which was expected due to the bands being closer to the Balmer jump. The rms of these residuals is always lower than 6% for both libraries.

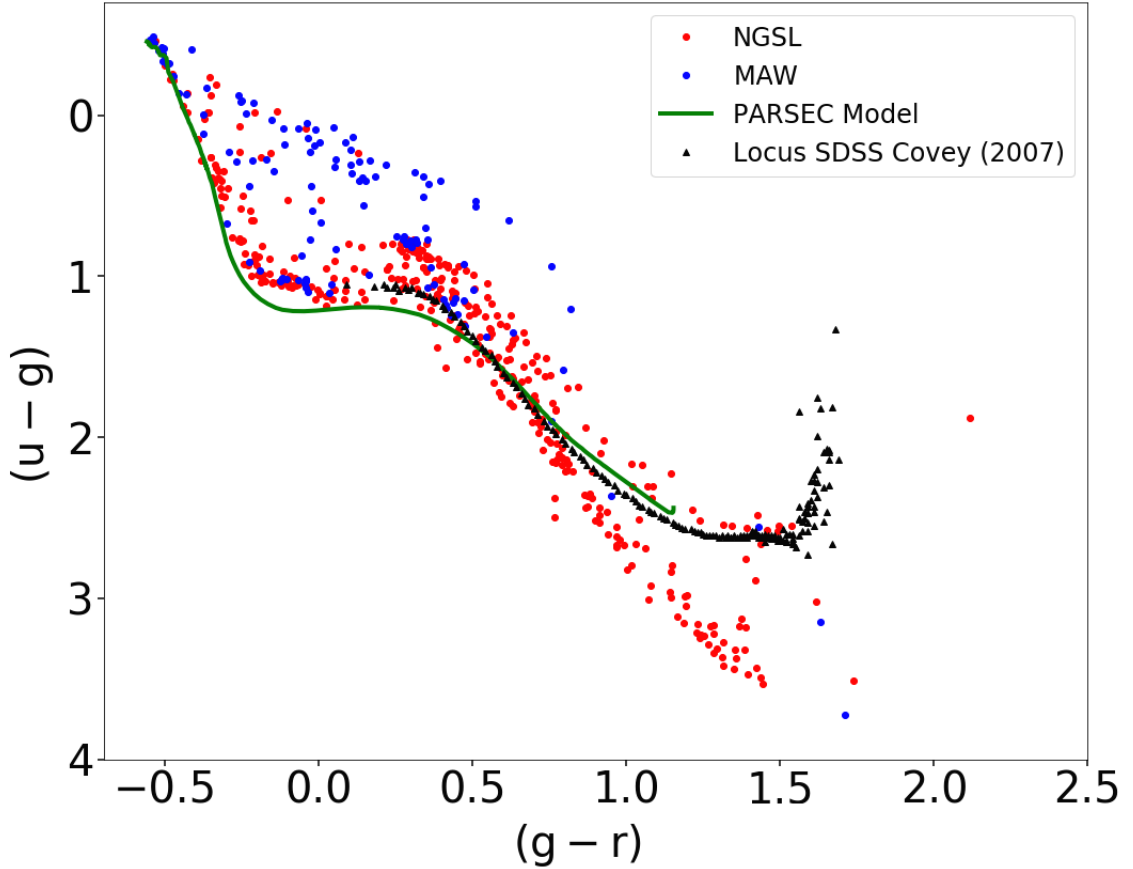


Figure 5. Colour-colour diagram using *SDSS* synthetic photometry for both catalogues. NGSL stars are red dots while MAW stars are shown as blue dots. We draw a 1 Myr theoretical PARSEC curve with solar metallicity and no extinction. Black triangles represent main stellar locus in *SDSS* photometry from Covey et al. (2007).

The relationship of NGSL residuals with temperature and reddening is shown more clearly in Figure 7. Here we have represented fitting residuals versus tabulated NGSL temperature together with its absorption in the visible range (A_V) marked by different colours (<https://archive.stsci.edu/prepds/stisngsl/>, Heap & Lindler (2016)). As can be seen, differences due to reddening are not very marked, since in all cases we are limited to values lower than 0.7. However, fitting these transformations by a single colour generates substructures in the residuals, such as those observed in filters F348M, F420N, F450N and F660N. Nonetheless, these transformation equations allow us to establish a first ZP of the GALANTE photometry, which will be very dependent on the *SDSS* data quality in the regions to be calibrated.

We also estimated the inverse transformation equations from GALANTE to *SDSS* following the same procedure. The results are shown in Equation 13.

$$\begin{aligned}
 u - F348M &= -0.149; \text{ rms} = 0.067 \\
 g - F515N &= 0.591 \cdot (F450N - F515N) + 0.025; \text{ rms} = 0.018 \\
 r - F665N &= 0.151 \cdot (F450N - F660N) - 0.013; \text{ rms} = 0.013 \\
 i - F861M &= 0.205 \cdot (F515N - F861M) - 0.055; \text{ rms} = 0.022 \\
 z - F861M &= -0.068 \cdot (F660N - F861M) - 0.005; \text{ rms} = 0.013
 \end{aligned}
 \tag{13}$$

5 CALIBRATION OF THE GALANTE PHOTOMETRY

5.1 CALIBRATION USING SDSS

In this section, we will calibrate the GALANTE photometry for a small region of Cyg OB2, applying transformation equations from Equation 12. These data have been obtained over the past 3 years through requests for open observation times from the Javalambre observatory. Data has been previously reduced by the CEFCA team, and aperture photometry has been obtained at the IAA.

We select DR8 and DR12 as possible sources for obtaining GALANTE ZPs through the transformation equations. DR8 has been selected because a previous Cyg OB2 study

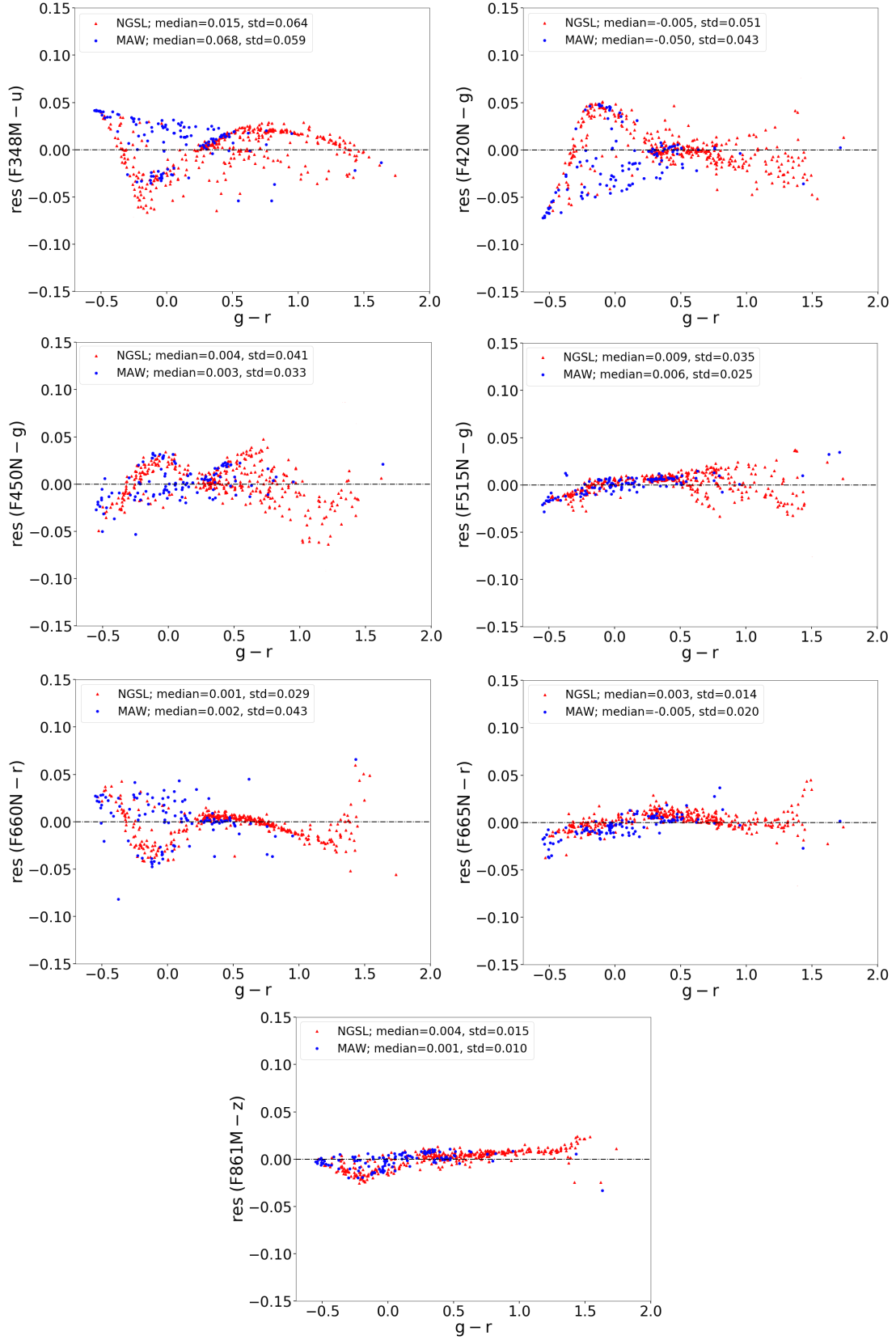


Figure 6. Residual fitting errors for both catalogues from Equation 12. NGSL stars are plotted in red dots and MAW stars are shown in blue dots.

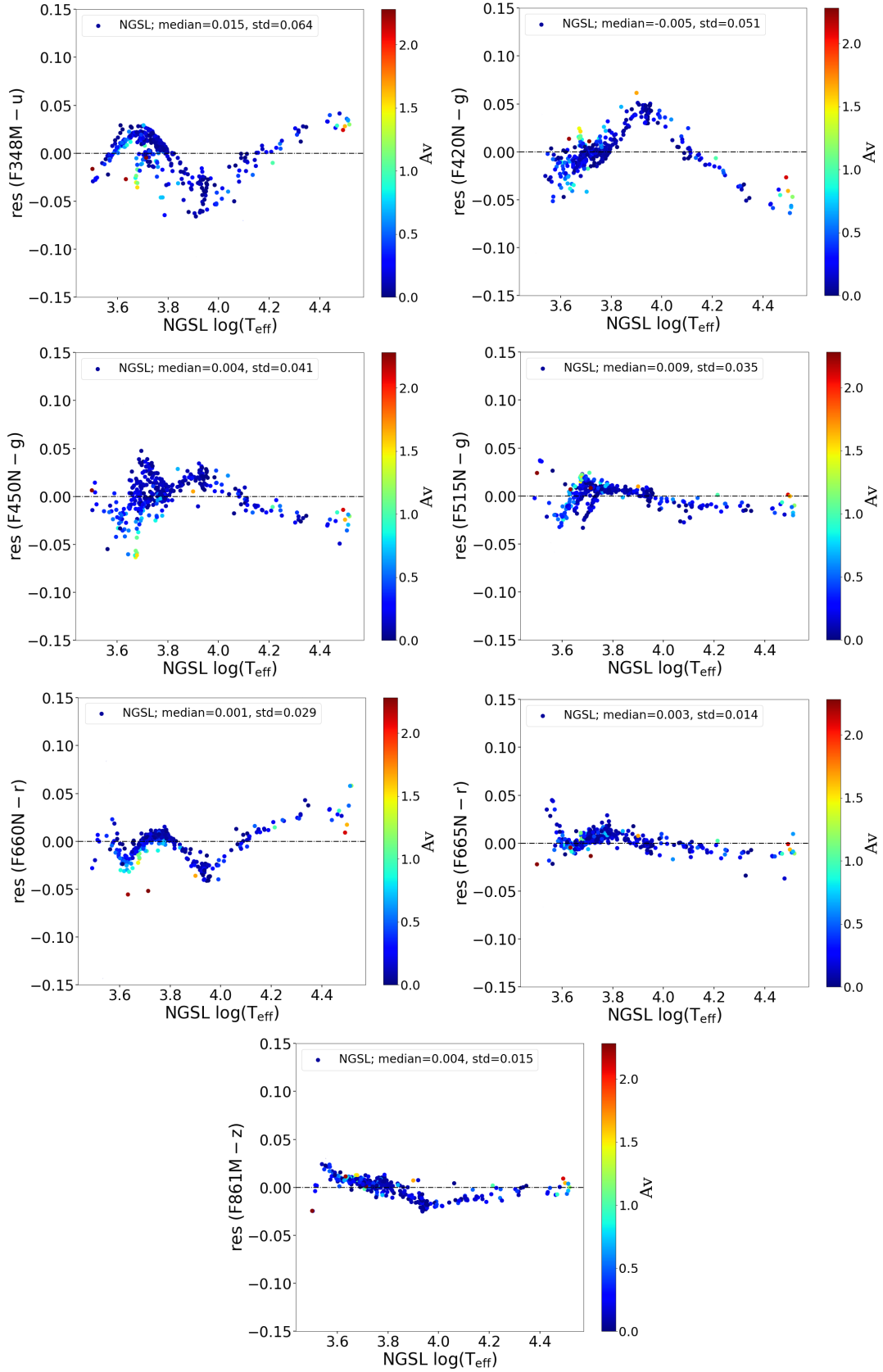


Figure 7. These plots show the residual errors from the fitting depending on the effective temperature and colour excess. The colour map scale represents A_V . Both stellar parameters are extracted from the NGSL library.

Table 4. GALANTE photometric ZPs from *SDSS* DR8 and DR12.

Band	ZP DR8	error DR8	ZP DR12	error DR12
F348M	26.046	0.004	26.058	0.004
F420N	24.365	0.006	24.349	0.005
F450N	24.496	0.005	24.482	0.005
F515N	26.443	0.004	26.433	0.004
F660N	25.905	0.004	25.907	0.004
F665N	24.057	0.006	24.058	0.006
F861M	26.427	0.003	26.427	0.003

by Guarcello et al. (2012) was based on this release, while our transformation is based on DR12. Thus we now want to compare both releases in order to see the ZP differences we can obtain using both catalogues.

Firstly, we directly compare *SDSS* photometry in both data releases taking common stars observed with the Javalambre Auxiliary Survey Telescope (hereinafter T-80 telescope). This crossmatch gives a total of 130 stars in Cyg OB2. Figure 8 represents the differences between both releases.

Figure 8 shows a significant difference in *u* and *g* bands for both releases, showing a light magnitude equation (green dots line) for these two bands. This effect was already known by the *SDSS* team and appeared to be due to the ubercalibration procedure described by Padmanabhan et al. (2008). DR12 was already corrected of this effect. Differences in *r*, *i*, and *z* bands are shown to be lower than a few thousandths of magnitudes and without any evidence of systematic effect. Nonetheless, even though we are observing an equation magnitude between both releases, differences between magnitudes show median values below one hundred, as seen in the histograms of Figure 8.

After this analysis, we decided to obtain GALANTE photometry ZPs based on both releases and comparing them afterward. Using both releases, we obtain the difference between GALANTE photometries shown in Figure 9, where we can see that the median and rms of these distributions are below 0.02 magnitudes for all bands. The final ZPs for each GALANTE band are shown in Table 4. Thus, we choose to calibrate GALANTE photometry with *SDSS* data release 12 before to analyze the calibration procedure with the new *RefCat2* catalogue.

5.2 CALIBRATION USING RefCat2

While we were writing this work, Tonry et al. (2018) published a new catalogue (*RefCat2*) with *griz* photometry of 993 million stars to $m < 19$. According to the authors, *RefCat2* has an internal precision of 0.02 mag for stars in the Galactic disk and is free of systematic effects. In accordance with these premises and at referee’s suggestion, we decided to obtain the GALANTE ZPs using this library, however, due to the lack of a *u* band in this catalogue, we have to continue using *u* from *SDSS* DR12. Attending to both libraries, we compare differences between these ZPs in Figure 10.

A clear fact to validate this catalogue is that, if these stars present lower systematic errors than those of *SDSS*

DR12, this should be translated into the ZP distribution (instrumental - catalogue) for each filter. Figure 11 represents GALANTE photometry histograms for these ZP differences comparing with *RefCat2* (in blue) and *SDSS* DR12 (in red). Two facts are clearly observed: *RefCat2* ZPs are more peaked than *SDSS* based ones, and they are also more symmetrical, without the large skews present in the *SDSS* distribution.

Tails that we observe in the ZPs from *SDSS* DR12, suggest the presence of systematic errors for the brightest stars in *SDSS* DR12, as seen in Figure 10. After this analysis, and considering that *RefCat2* is an all-sky survey, we consider *RefCat2* our base catalogue to obtain the preliminary calibration of the GALANTE photometric system.

As an example of the obtained results using *RefCat2*, we have drawn the bracket diagram of Figure 4 for our Cyg OB2 field. The results are shown in Figure 12, where the main and giant sequences by Kurucz as listed by Castelli et al. (1997) are also overplotted. We selected Kurucz ODFNEW/NOVER theoretical spectra to obtain the GALANTE synthetic photometry. Kurucz’s library provides a coverage of $3500 \text{ K} \leq T_{\text{eff}} \leq 50000 \text{ K}$ (in steps of 200 K below $T_{\text{eff}} = 13000 \text{ K}$, and 1000 K otherwise), $0.0 \leq \log(g) \leq 5.0$ (in steps of 0.5 dex) and $-2.5 \leq [\text{Fe}/\text{H}] \leq 0.5$ (in steps of 0.2 and 0.5). These low-resolution spectra are sampled from 90.9 \AA to $160 \mu\text{m}$, which includes the GALANTE wavelength range. Solar metallicity, reddening free lines (main sequence: black, and giant: red) are shown.

We observe that most stars are arranged between the two main lines (main sequence and giant stars) and that the most scattered ones could be dispersed due to high variable reddening and/or ZP error propagation. However, the observed stellar distribution in this plot produces confidence in our ZP choice as a preliminary calibration of the GALANTE photometry. We will compare this calibration with a more sophisticated one in a following paper where we will present the GALANTE photometry of Cyg OB2.

6 CONCLUSIONS

We present the characterization of the GALANTE photometric system as defined by the convolution of four different response functions: atmosphere, filter, detector, and mirror. The set of primary standard stars to define the GALANTE photometric system is composed of the 378 stars from NGSL library, which cover a wide range of spectral types, luminosity classes and metallicities. We enhance it with the MAW library, which provides a sample of 122 stars. Both libraries provide 500 GALANTE spectrophotometric standard stars. Using this compilation to obtain the GALANTE and *SDSS* synthetic photometries in the AB system, we derive transformation equations from *SDSS* photometry to the GALANTE photometric system (and vice versa) using the BIC parameter as a figure of merit for selecting the best model.

Figure 6 shows that a simple *SDSS* model (band+colour; Equation 12) is able to shape the GALANTE system up to an rms level of 0.06 magnitudes in the worst case. It is worth noting that our compiled final library covers a wide range of effective temperature, $\log(g)$, metallicity, and, most importantly, reddening. This means that our transformations, despite the noise, can be considered as

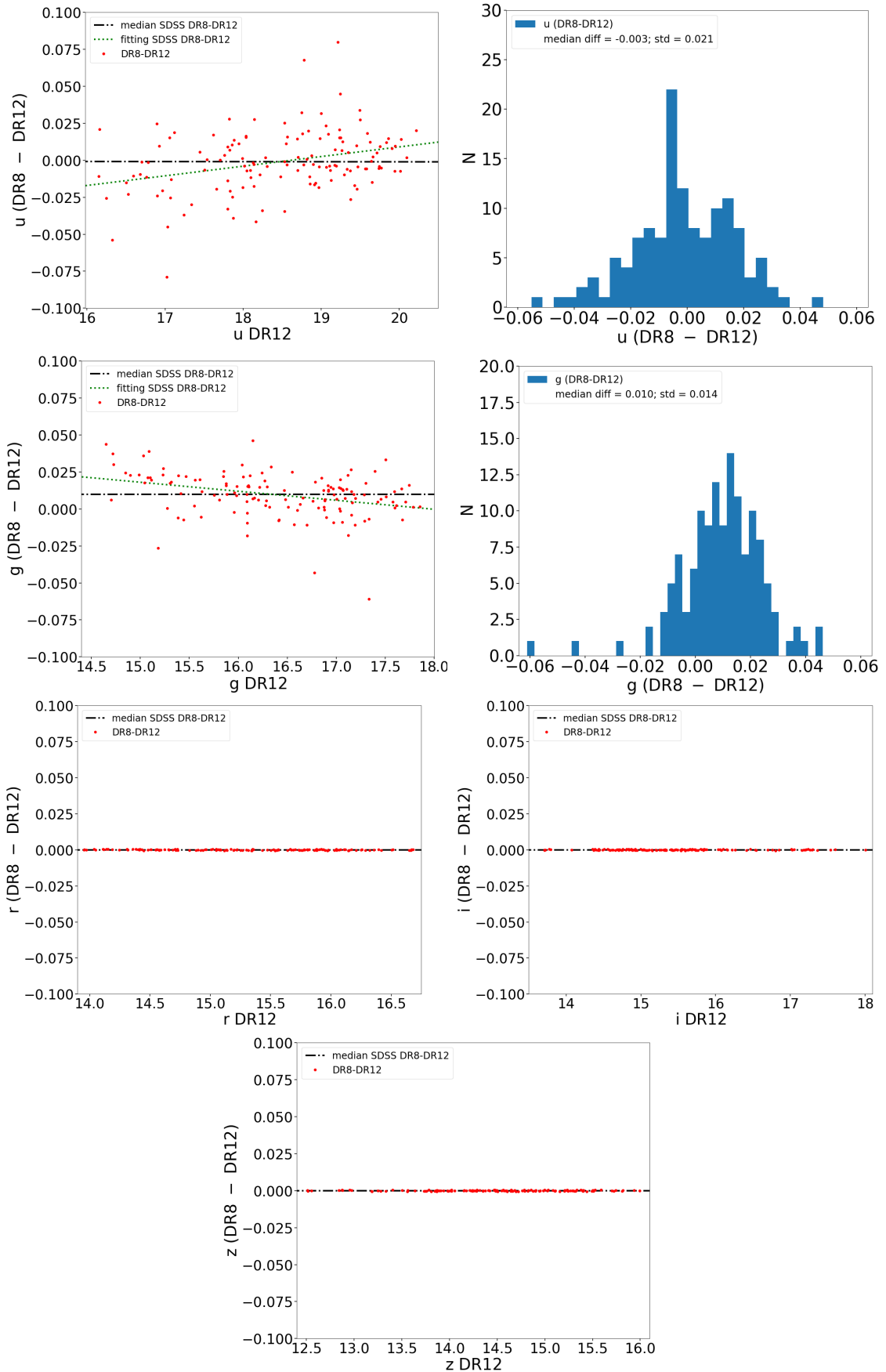


Figure 8. These figures represent differences for stars observed with the Javalambre observatory T-80 telescope in Cyg OB2 and their *SDSS* photometry taken directly from DR8 and DR12.

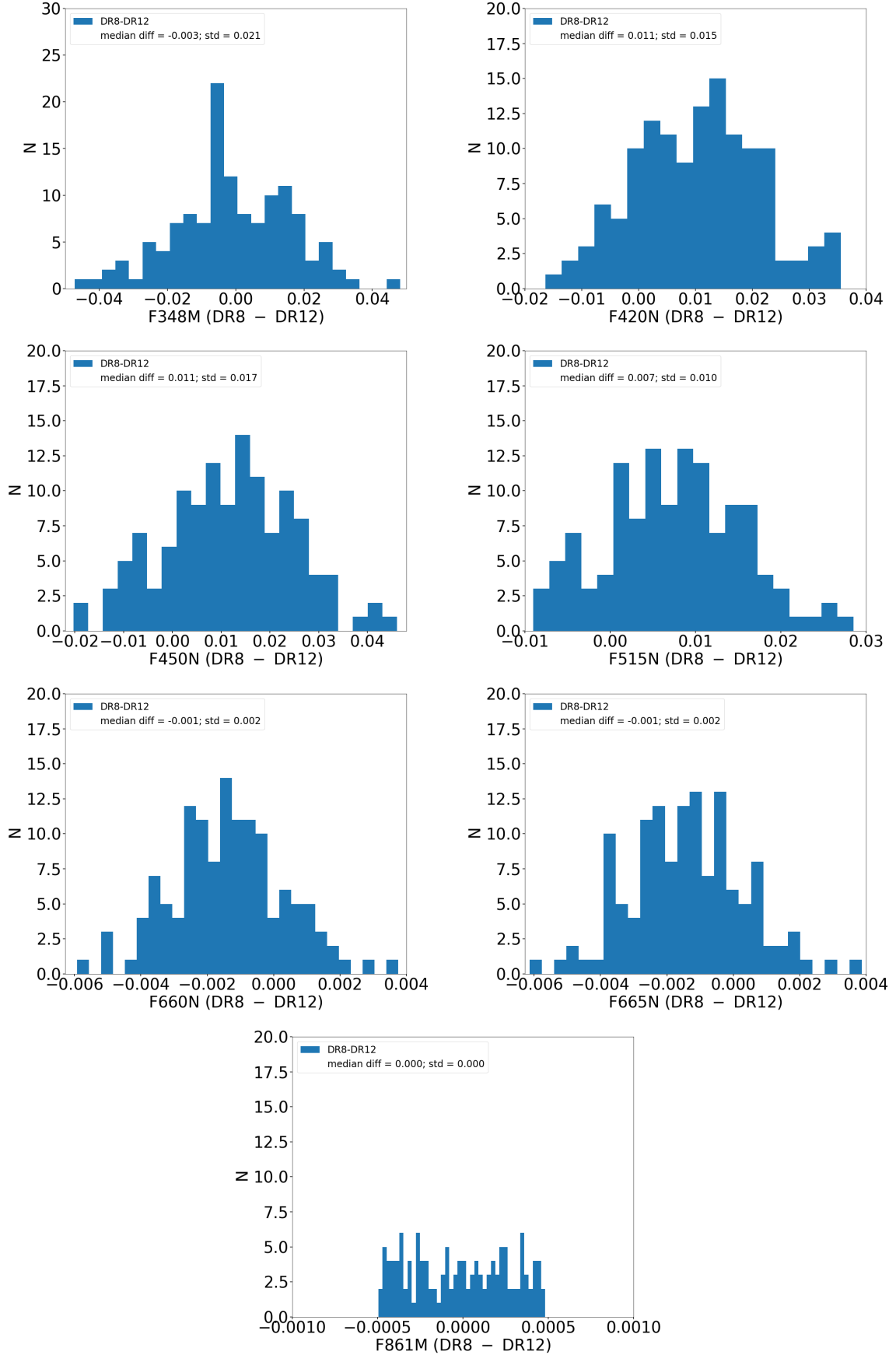


Figure 9. GALANTE photometry histograms for differences between *SDSS* DR8 and DR12 using a small region of Cyg OB2 observed by the T-80 telescope.

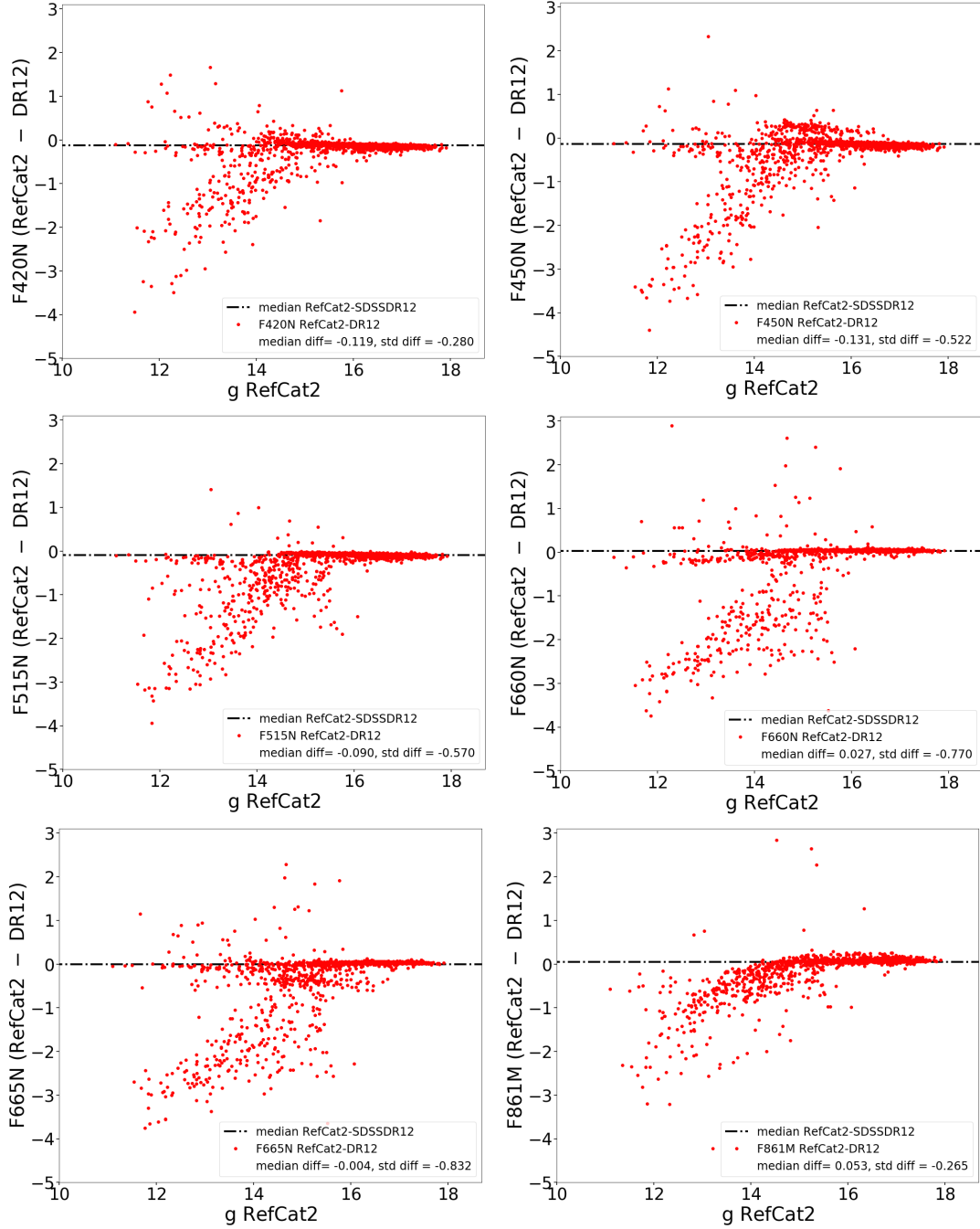


Figure 10. These figures represent differences for stars observed with the Javalambre observatory T-80 telescope in Cyg OB2 and their *RefCat2* and *SDSS DR12* photometry taken directly from both libraries.

unbiased. This point is better observed in Figure 7, where only NGSL stars are plotted and their dependence on temperature and reddening show a rippled way but limited to an amplitude lower than 0.05 magnitude.

We use Equation 12 to obtain the GALANTE photometric ZPs in a field of Cyg OB2 observed using the Javalambre observatory. The ZPs have been obtained from *SDSS DR8* and *DR12* releases. Despite the *u* and *g* magnitude equations between both data releases, the ZP difference is always below 0.01 with an rms of the order of 0.02. During our work, a new *griz* catalogue called *RefCat2* from

Tomry et al. (2018) was published. However, the observed stellar distribution of this new catalogue, covering the whole sky, represents an excellent choice for the preliminary calibration of the GALANTE photometry, if, as its authors proclaim, the average internal precision is 0.02 magnitudes for the stars of the Galactic disk and is free of systematic effects. We have made a comparison between the ZPs obtained from *SDSS DR12* and *RefCat2*, finding that the distribution of the ZPs derived from *RefCat2* shows a better behavior, with more centralized values and shorter tails (see Figures 10 and 11). For this reason we adopted *RefCat2* as

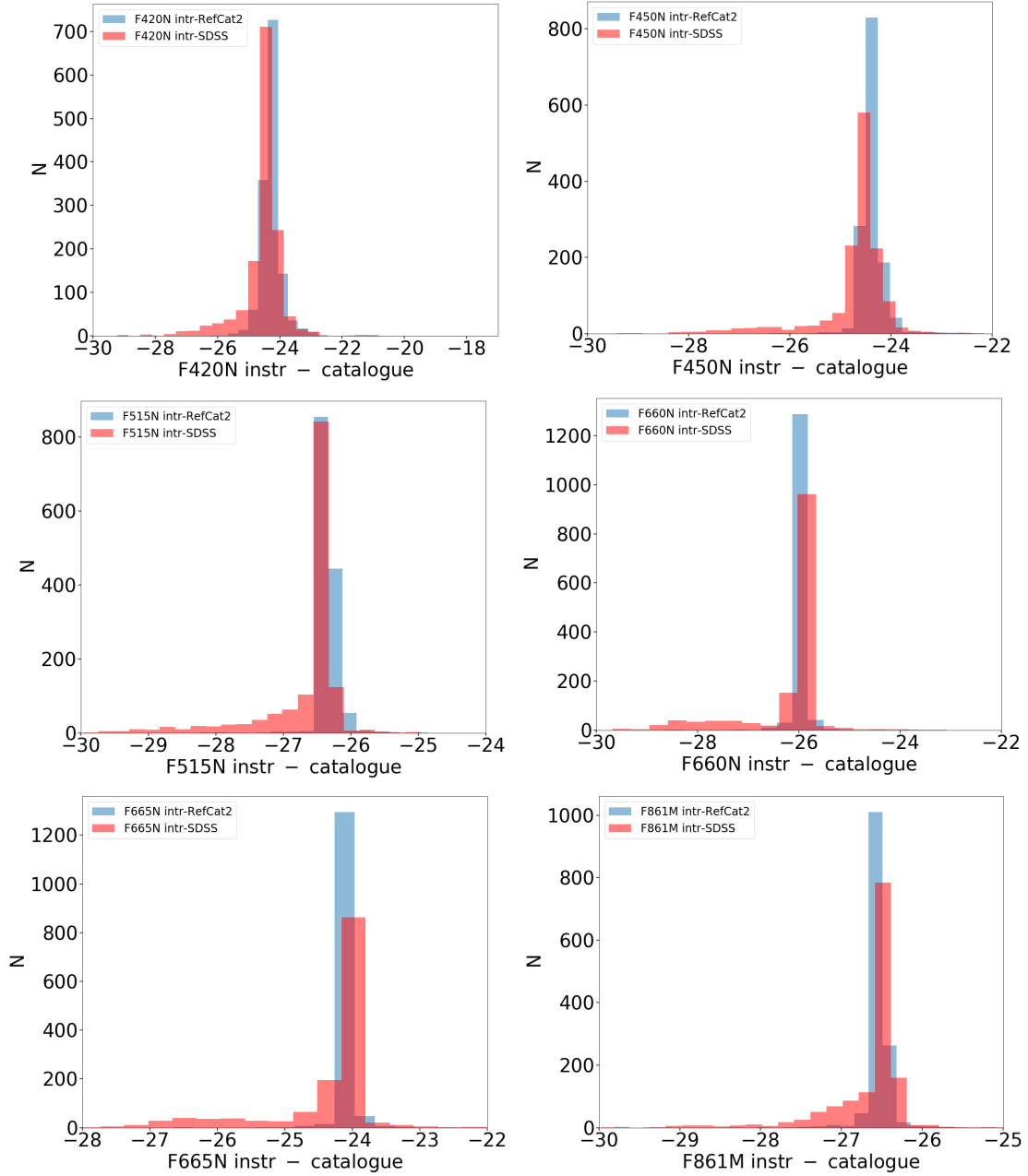


Figure 11. GALANTE photometry histograms for differences between instrumental AB magnitudes minus *RefCat2* (in blue) and *SDSS* DR12 (in red) using a small region of Cyg OB2 observed by the T-80 telescope.

the base catalogue for GALANTE calibration. The application of the *RefCat2* ZPs to our photometry is shown in Figure 12, where the Kurucz’s fiducial lines corresponding to main sequence and giant stars of solar metallicity are also overplotted. The agreement between the observed photometry and the theoretical tracks means that we are confident in this ZP calibration. In our next paper, we will compare this calibration with another more complex procedure for a final analysis of the GALANTE photometry of the Cyg OB2 association.

ACKNOWLEDGEMENTS

We would like to thank the referee, Prof. Bessell, for his invaluable comments and suggestions, helping us to improve the presentation of our results. We thank the Centro de Estudios de Física del Cosmos de Aragón (CEFCA) team in Teruel and Javalambre for supporting us in this project, giving us the opportunity to use non-J-PLUS useful nights to develop the GALANTE survey. We also want to recognize the work of the NGSL team (Gregg et al. 2006; Heap & Lindler 2016) whose observational catalogue has been of great help for our work. This research made use of Python (<http://www.python.org>); Numpy (van der Walt et al. 2011); Scipy (Jones et al. 2001); and Matplotlib

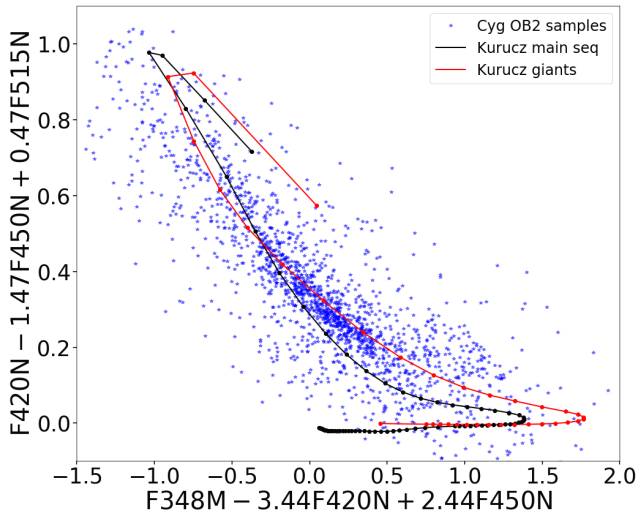


Figure 12. Bracket diagram using GALANTE filter set similar to Figure 4. It shows only tracks with solar metallicity models with $\log(g)=4.5$ (black line) and $\log(g)=2.5$ (red line). We represent Cyg OB2 calibrated samples for this work by blue star-shapes.

(Hunter 2007), a suite of open-source python modules that provides a framework for creating scientific plots. We also acknowledge the use of STILTS and TOPCAT tools Taylor (2005). A.L.-G, E.J.A, and J.M.A. acknowledge support from the Spanish Government Ministerio de Ciencia, Innovación y Universidades through grants AYA2013-40 611-P and AYA2016-75 931-C2-1/2-P. A.L.-G and E.J.A also acknowledge support from the State Agency for Research of the Spanish MCIU through the "Center of Excellence Severo Ochoa" award for the Instituto de Astrofísica de Andalucía (SEV-2017-0709).

This paper has been typeset from a $\text{T}_{\text{E}}\text{X}/\text{L}^{\text{A}}\text{T}_{\text{E}}\text{X}$ file prepared by the author.

REFERENCES

- Aparicio Villegas T., et al., 2010, *AJ*, **139**, 1242
- Becker W., 1946, *Veröffentlichungen der Universitaets-Sternwarte zu Goettingen*, **5**, 159
- Benitez N., et al., 2014, arXiv e-prints,
- Bessell M. S., 2011, *PASP*, **123**, 1442
- Bohlin R. C., 2007, in Sterken C., ed., *Astronomical Society of the Pacific Conference Series Vol. 364, The Future of Photometric, Spectrophotometric and Polarimetric Standardization*. p. 315 (arXiv:astro-ph/0608715)
- Casagrande L., VandenBerg D. A., 2014, *MNRAS*, **444**, 392
- Castelli F., Gratton R. G., Kurucz R. L., 1997, *A&A*, **318**, 841
- Cenarro A. J., J-PAS Collaboration J-PLUS Collaboration 2017, in *Highlights on Spanish Astrophysics IX*. pp 11–19
- Cenarro A. J., J-PAS Collaboration J-PLUS Collaboration 2018, *Commissioning and first scientific operations of the wide-field 2.6m Javalambre Survey Telescope*, doi:10.1117/12.2309520
- Covey K. R., et al., 2007, *AJ*, **134**, 2398
- Evans D. W., et al., 2018, *A&A*, **616**, A4
- Fukugita M., Ichikawa T., Gunn J. E., Doi M., Shimasaku K., Schneider D. P., 1996, *AJ*, **111**, 1748
- Gaia Collaboration et al., 2018, *A&A*, **616**, A1
- Golay M., ed. 1974, *Introduction to astronomical photometry Astrophysics and Space Science Library Vol. 41*, doi:10.1007/978-94-010-2169-2.
- Gregg M. D., et al., 2006, in Koekemoer A. M., Goudfrooij P., Dressel L. L., eds, *The 2005 HST Calibration Workshop: Hubble After the Transition to Two-Gyro Mode*. p. 209
- Guarcello M. G., Wright N. J., Drake J. J., García-Alvarez D., Drew J. E., Aldcroft T., Kashyap V. L., 2012, *ApJS*, **202**, 19
- Heap S. R., Lindler D., 2016, in Deustua S., Allam S., Tucker D., Smith J. A., eds, *Astronomical Society of the Pacific Conference Series Vol. 503, The Science of Calibration*. p. 211
- Hunter J. D., 2007, *Computing In Science & Engineering*, **9**, 90
- Johnson H. L., Morgan W. W., 1953, *ApJ*, **117**, 313
- Jones E., Oliphant T., Peterson P., et al., 2001, *SciPy: Open source scientific tools for Python*, <http://www.scipy.org/>
- Koleva M., Vazdekis A., 2012, *A&A*, **538**, A143
- Maíz Apellániz J., 2013, in Guirado J. C., Lara L. M., Quilis V., Gorgas J., eds, *Highlights of Spanish Astrophysics VII*. pp 657–657 (arXiv:1209.1709)
- Maíz Apellániz J., 2017, in *Early Data Release and Scientific Exploitation of the J-PLUS Survey*, held 2-3 October 2017 in Teruel, Spain, Online at <http://riastronomia.es/en/early-data-release-and-scientific-exploitation-of-the-j-plus-survey/> id. 15. p. 15, doi:10.5281/zenodo.1040919
- Maíz Apellániz J., Barbá R. H., 2018, *A&A*, **613**, A9
- Maíz Apellániz J., Sota A., 2008, in *RMxAC*. pp 44–46
- Maíz Apellániz J., Weiler M., 2018, *A&A*, **619**, A180
- Maíz Apellániz J., et al., 2014, *A&A*, **564**, A63
- Marigo P., et al., 2017, *ApJ*, **835**, 77
- McClure R. D., van den Bergh S., 1968, *AJ*, **73**, 313
- Oke J. B., Gunn J. E., 1983, *ApJ*, **266**, 713
- Padmanabhan N., et al., 2008, *ApJ*, **674**, 1217
- Saito R. K., Minniti D., de Oliveira C. M., 2018, in Chiappini C., Minchev I., Starkenburg E., Valentini M., eds, *IAU Symposium Vol. 334, Rediscovering Our Galaxy*. pp 358–359, doi:10.1017/S1743921317007025
- Smith J. A., et al., 2002, *AJ*, **123**, 2121
- Strömgren B., 1966, *ARA&A*, **4**, 433
- Taylor M. B., 2005, in Shopbell P., Britton M., Ebert R., eds, *Astronomical Society of the Pacific Conference Series Vol. 347, Astronomical Data Analysis Software and Systems XIV*. p. 29
- Tokunaga A. T., Vacca W. D., 2005, *PASP*, **117**, 1459
- Tonry J. L., et al., 2018, *ApJ*, **867**, 105
- Walraven T., Walraven J. H., 1960, *Bull. Astron. Inst. Netherlands*, **15**, 67
- Weiler M., 2018, *A&A*, **617**, A138
- van der Walt S., Colbert S. C., Varoquaux G., 2011, *Computing in Science and Engineering*, **13**, 22